Visible Absorption Spectrum of the CH_3CO Radical

B. Rajakumar,[†,‡] Jonathan E. Flad,[†,‡] Tomasz Gierczak,[†,‡,§] A. R. Ravishankara,[†,#] and James B. Burkholder*[,†]

Earth System Research Laboratory, Chemical Sciences Division, National Oceanic and Atmospheric Administration, 325 Broadway, Boulder, Colorado 80305-3328, and Cooperative Institute for Research in Environmental Sciences, University of Colorado, Boulder, Colorado 80309

Received: May 1, 2007; In Final Form: June 20, 2007

The visible absorption spectrum of the acetyl radical, CH_3CO, was measured between 490 and 660 nm at 298 K using cavity ring-down spectroscopy. Gas-phase CH_3CO radicals were produced using several methods including: (1) 248 nm pulsed laser photolysis of acetone ($CH_3C(O)CH_3$), methyl ethyl ketone (MEK, $CH_3C(O)CH_2CH_3$), and biacetyl ($CH_3C(O)C(O)CH_3$), (2) $Cl + CH_3C(O)H \rightarrow CH_3C(O) + HCl$ with Cl atoms produced via pulsed laser photolysis or in a discharge flow tube, and (3) $OH + CH_3C(O)H \rightarrow CH_3CO + H_2O$ with two different pulsed laser photolysis sources of OH radicals. The CH_3CO absorption spectrum was assigned on the basis of the consistency of the spectra obtained from the different CH_3CO sources and agreement of the measured rate coefficients for the reaction of the absorbing species with O_2 and O_3 with literature values for the $CH_3CO + O_2 + M$ and $CH_3CO + O_3$ reactions. The CH_3CO absorption spectrum between 490 and 660 nm has a broad peak centered near 535 nm and shows no discernible structure. The absorption cross section of CH_3CO at 532 nm was measured to be $(1.1 \pm 0.2) \times 10^{-19}$ cm^2 molecule^{-1} (base e).

1. Introduction

The acetyl radical, CH_3CO, is an important intermediate in tropospheric hydrocarbon oxidation chemistry. The CH_3CO radical is formed in the atmosphere in several ways including the reactions of OH with $CH_3C(O)H$ and $CH_3C(O)C(O)H$ and as a primary product in the UV photolysis of carbonyl compounds such as acetone ($CH_3C(O)CH_3$), methyl ethyl ketone (MEK, $CH_3C(O)CH_2CH_3$), biacetyl ($CH_3C(O)C(O)CH_3$), methylglyoxal ($CH_3C(O)C(O)H$), and acetyl halides. In the atmosphere, the CH_3CO radical is rapidly converted to the acetylperoxy radical via its reaction with O_2[1,2]

$$CH_3CO + O_2 + M \rightarrow CH_3C(O)O_2 + M \qquad (1)$$

The acetylperoxy radical, in turn, leads to the formation of peroxyacetyl nitrate (PAN, $CH_3C(O)O_2NO_2$)

$$CH_3C(O)O_2 + NO_2 + M \leftrightarrow CH_3C(O)O_2NO_2 + M \qquad (2,-2)$$

an important atmospheric reservoir for NO_x ($NO + NO_2$).[3]

The photochemistry of carbonyl compounds has been studied extensively over the years. Special focus has been placed on the photochemistry of acetone

$$CH_3C(O)CH_3 + h\nu \rightarrow \text{products} \qquad (3)$$

because it can be a significant source of HO_x ($HO_x = OH + HO_2$) in the troposphere.[4,5] A number of experimental methods have been used in these studies with recent work utilizing in situ detection of CH_3,[6] CO,[7] and OH[8,9] (OH is produced via the reaction of CH_3CO with O_2). Other studies have monitored acetone loss or analyzed stable end-products[10−14] to determine quantum yields for loss of acetone or formation of specific products. Further details of acetone photochemistry, such as the pressure and temperature dependence of its photolysis quantum yields, are needed for accurate atmospheric modeling, particularly at wavelengths >290 nm. Direct detection of the CH_3CO radical, a primary acetone photolysis product, via a sensitive optical technique such as cavity ring-down spectroscopy (CRDS), as described in this work, would greatly aid studies of acetone photochemistry.

The electronic spectroscopy of the CH_3CO radical, in contrast to the similar HCO radical (see Flad et al.[15] and references cited within), is currently not well characterized. Mao et al.[16] report ab initio calculations for the four lowest lying excited electronic states of CH_3CO. Vertical transition energies from the X^2A' ground state to the A^2A'', B^2A', C^2A', and D^2A'' excited states were found to be 60 (476 nm), 113 (253 nm), 154.5 (185 nm), and 161.4 (177 nm), respectively, in units of kcal mol^{-1} (wavelength). The CH_3CO UV absorption spectrum has been measured experimentally and found to be continuous with a peak absorption cross section in the range $(1.07-1.5) \times 10^{-17}$ cm^2 molecule^{-1} near 215 nm.[17,18] Theoretically, the transition from the ground X^2A' state to the lowest excited state, A^2A'', of CH_3CO which was calculated to be bound, falls in the visible wavelength region. The location, structure, and absorption strength of the $A^2A'' \leftarrow X^2A'$ transition for the CH_3CO radical has not been determined experimentally to date. The transition to the A^2A'' state in HCO, for comparison, leads to an absorption spectrum that extends over the wavelength range 450−900 nm, with highly resolvable ro-vibrational structure. To our knowledge, the only attempt to observed the $A^2A'' \leftarrow X^2A'$ transition for the CH_3CO radical was by Li et al.[16,19] However, their attempts to detect CO infrared emission (CO is possibly

* Corresponding author. E-mail: James.B.Burkholder@noaa.gov.
† National Oceanic and Atmospheric Administration.
‡ University of Colorado.
§ Permanent address: Department of Chemistry, Warsaw University, ul. Zwirki i Wigury 101, 02-089, Warsaw, Poland.
# Also associated with the Department of Chemistry and Biochemistry, University of Colorado, Boulder, CO 80309.

10.1021/jp073339h CCC: $37.00
Published on Web 08/18/2007

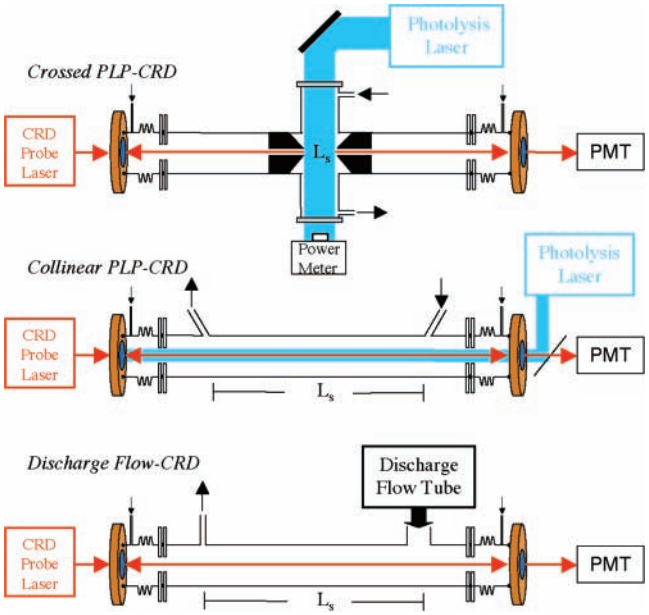

Figure 1. Schematics of the experimental setups used in the present study. The different setups couple a cavity ring-down cell with various methods for CH_3CO radical production that include crossed pulsed laser photolysis, collinear pulsed laser photolysis, and discharge fast flow. The smaller arrows indicate the gas flows that purge the CRD mirrors, and the larger arrows show the direction of gas flow for the reaction mixtures. L_s is the path length of the absorbing species.

produced as a photoproduct of the CH_3CO excitation to the A^2A'' state) were unsuccessful. On the basis of these measurements and results from their theoretical calculations, they conclude that the A^2A'' state is bound.

In this paper, we report the visible absorption spectrum of the acetyl radical, CH_3CO, over the wavelength range 490−660 nm. Spectra were measured using cavity ring-down spectroscopy (CRDS) at 298 K following CH_3CO formation from five different reaction and photolytic sources. In addition, the rate coefficients of the reaction of the absorbing species (CH_3CO) with O_2 and O_3 were measured and compared with literature values[1,2,20] to help confirm the identity of the absorbing species. Absolute absorption cross sections for the $A^2A'' \leftarrow X^2A'$ transition between 490 and 660 nm were determined using the reaction

$$OH + CH_3C(O)H \rightarrow CH_3CO + H_2O \qquad (4)$$

to produce CH_3CO with a calibrated initial OH radical concentration.

2. Experimental Details

The objective of this work was not only to measure the visible absorption spectrum of the CH_3CO radical but also to confirm that the measured spectrum was indeed due to the CH_3CO radical. To accomplish these goals, multiple methods were used to produce the CH_3CO radical and quantify its absorption cross sections. In addition, the rate coefficient for the reaction of the absorbing species (CH_3CO) with O_2 and O_3 were measured and compared with available literature values to confirm the identity of the absorbing species.

Cavity ring-down spectroscopy (CRDS) was used to measure the transient absorption signal of the CH_3CO radical following its production via pulsed laser photolysis (PLP) or in a discharge flow reactor. Details of the cavity ring-down technique are available elsewhere.[15,21−23] The experimental apparatus used in this work are shown schematically in Figure 1. The experimental configurations used include two PLP setups, one where the CRD and the photolysis laser beams were collinear and another where the two beams crossed at a right angle. A third configuration coupled the CRD optical cavity with a discharge fast-flow reactor. Experimental details specific to the present work dealing with the (1) CH_3CO radical sources, (2) cavity ring-down measurements, (3) rate coefficient measurements for the reactions of CH_3CO with O_2 and O_3, and (4) the determination of the CH_3CO absorption cross sections are described in the following sections.

2.1. CH_3CO Radical Sources. Reactions 3−7 were used to produce gas-phase CH_3CO radicals.

$$CH_3C(O)CH_3 + h\nu \rightarrow CH_3CO + CH_3 \qquad \lambda_T = 338 \text{ nm} \quad (3a)$$

$$\rightarrow 2CH_3 + CO \qquad \lambda_T = 298 \text{ nm} \quad (3b)$$

$$OH + CH_3C(O)H \rightarrow H_2O + CH_3CO \qquad \Delta_rH^0 = -29.4 \text{ kcal mol}^{-1} \quad (4a)$$

$$\rightarrow H_2O + CH_2C(O)H \qquad \Delta_rH^0 = -24.5 \text{ kcal mol}^{-1} \quad (4b)$$

$$Cl + CH_3C(O)H \rightarrow HCl + CH_3CO \qquad \Delta_rH^0 = -13.7 \text{ kcal mol}^{-1} \quad (5a)$$

$$\rightarrow HCl + CH_2C(O)H \qquad \Delta_rH^0 = -8.8 \text{ kcal mol}^{-1} \quad (5b)$$

$$CH_3C(O)CH_2CH_3 + h\nu \rightarrow CH_3CO + CH_3CH_2 \qquad \lambda_T = 342 \text{ nm} \quad (6a)$$

$$\rightarrow CH_3 + CH_3CH_2CO \qquad \lambda_T = 323 \text{ nm} \quad (6b)$$

$$\rightarrow CH_3 + CO + CH_3CH_2 \qquad \lambda_T = 302 \text{ nm} \quad (6c)$$

$$CH_3C(O)C(O)CH_3 + h\nu \rightarrow 2CH_3CO \qquad \lambda_T = 390 \text{ nm} \quad (7a)$$

$$\rightarrow CH_3CO + CO + CH_3 \qquad \lambda_T = 338 \text{ nm} \quad (7b)$$

$$\rightarrow 2CH_3 + 2CO \qquad \lambda_T = 300 \text{ nm} \quad (7c)$$

The standard heats of reaction, Δ_rH^0, and the photolysis thresholds, λ_T, at 298 K were calculated using thermochemical data taken from Sander et al.[24] and the NIST Chemistry webbook.[25] Reactions 4a and 5a are good sources of the CH_3CO radical owing to their large reaction rate coefficients, $k_4(298\text{ K}) = 1.4 \times 10^{-11}$ cm^3 molecule^{-1} s^{-1}[24] and $k_5(298\text{ K}) = 7.9 \times 10^{-11}$ cm^3 molecule^{-1} s^{-1}, and high yields for the CH_3CO radical; CH_3CO yields in reactions 4 and 5 are 0.95 (+0.017/−0.024)[18,26] and unity, respectively.[27,28] The pulsed laser photolysis sources that were used to produce CH_3CO in this study are also well suited for identifying the absorption spectrum of the CH_3CO radical. Although reactions 3, 6, and 7 have multiple photolysis channels energetically accessible, the CH_3CO yields at 248 nm are expected to be significant. For the purposes of this study reactions 3b, 6c, and 7b,c are written as single step (concerted) reactions. Measurements of the CH_3CO quantum yield from the 248 nm photolysis of acetone, MEK, and biacetyl

obtained during the course of this work are described elsewhere.[29] Other possible photoproducts in reactions 3, 6, and 7 include CO and the CH_3, CH_3CH_2, and CH_3CH_2CO radicals. CH_3 and CH_3CH_2, do not absorb in the visible region of the spectrum and, therefore, do not interfere with the determination of the CH_3CO visible absorption spectrum. The CH_3CH_2CO radical may be formed in the photolysis of MEK and its possible influence on the interpretation of the measured spectra is addressed in the Results and Discussion section.

2.2. Cavity Ring-Down Apparatus. The measured ring-down time constant, τ, is related to the absorption coefficient, $\alpha(\lambda)$ (cm^{-1}) by

$$\alpha(\lambda) = [A]\sigma_A(\lambda) = \frac{1}{c}\frac{d}{L_s}\left(\frac{1}{\tau(\lambda)} - \frac{1}{\tau_0(\lambda)}\right) \qquad (8)$$

where λ is the CRD probe wavelength, A is the absorbing species, $\sigma_A(\lambda)$ is the absorption cross section (cm^2 $molecule^{-1}$) of A at wavelength λ, d is the optical cavity path length (cm), L_s is the path length (cm) of the absorbing sample, c is the speed of light, and $\tau(\lambda)$ and $\tau_0(\lambda)$ are the ring-down time constants (s) with and without the absorber present, respectively. The pulsed laser beam for CRD measurements was taken from a frequency doubled Nd:YAG laser (532 nm), a Nd:YAG pumped dye laser (600−650 nm), or a 308 nm excimer pumped dye laser (490−660 nm). Light exiting the rear mirror of the optical cavity was collected with a fiber optic and detected using a photomultiplier tube. The output of the photomultiplier tube was collected and averaged on a 16 bit waveform digitizer card at a sample rate of 1 or 2 MHz. The wavelength of the dye laser output was measured using a commercial laser wavelength meter (wavelengths reported in this paper are in air). The linewidth of the dye laser light was ~0.1 cm^{-1} (Nd:YAG pumped) and ~0.4 cm^{-1} (excimer pumped). The linewidth of the frequency doubled Nd:YAG laser was ~1.4 cm^{-1}. CRD measurements were performed at various probe wavelengths at a fixed time delay after the pulsed laser (spectrum and cross section determinations) or with variable time delay (spectrum and rate coefficient determinations).

CRD measurements are commonly limited to a narrow range of wavelengths owing to the narrow bandwidth of CRD mirrors. Therefore, to measure the broad absorption spectra, 490−660 nm, of the CH_3CO radical using CRDS, multiple sets of highly reflective cavity mirrors were used. CRD measurements were typically made over a wavelength range ±15 nm of the maximum in mirror reflectivity. Scans were performed over these wavelength regions by stepping the wavelength of the probe dye laser in increments of 0.1 or 0.5 nm (the measured spectrum showed no resolvable structure and was independent of the step size). Five sets of mirrors were used to cover the wavelength range 490−660 nm. The reflectivity of the mirrors differed from one set to another. Values for τ_0 ranged from 30 to 120 μs for a cavity length of 1 m.

2.2.1. Crossed Pulsed Laser Photolysis−Cavity Ring-Down Setup. This setup was used for the majority of the experiments. Experiments included the determinations of the CH_3CO absorption spectrum, rate coefficients for the reactions of CH_3CO with O_2 and O_3, and CH_3CO absorption cross sections. A schematic of the apparatus is shown in Figure 1.

In this setup, the laser photolysis beam passed through the reaction cell at a right angle to the CRD optical cavity. The reactor, mounted midway between the CRD mirrors, was a 25 cm long 5 cm diameter Pyrex tube with 248 nm AR coated windows and side-arms to allow the CRD beam to pass through its center. Gas mixtures entered at one end of the reactor and flowed the length of the reactor and exited in front of the exit window. The photolysis beam was parallel to the gas flow, and the probe beam was orthogonal to the gas flow. The CRD probe beam was taken from either a frequency doubled Nd:YAG laser (532 nm) or a 308 nm excimer pumped dye laser (490−660 nm).

CH_3CO radicals were produced by the pulsed laser photolysis of the various precursors outlined above. The photolysis laser fluence was monitored continuously using a power meter mounted at the exit of the reactor that was calibrated using two independent methods described below. The photolysis beam filled the width of the reactor uniformly and was 2.5 cm high (much larger than the CRD beam diameter). The average power of the photolysis beam along the CRD absorption path, L_s, was measured to be constant to within ±10%. Over the course of the study, the laser fluence was varied over the range 3−15 mJ cm^{-2} $pulse^{-1}$ and the CH_3CO radical concentration was in the range $(1-4) \times 10^{12}$ molecule cm^{-3}. Baffles mounted in the reactor side-arms provided isolation of the CRD mirrors and minimized the scattered photolysis laser light reaching the CRD mirrors. The baffles also precisely defined the length of the optical path of the absorbing species, L_s.

In this crossed beam configuration, the CRD path length for the absorbing species is only a fraction of the total optical path length. The path length for the absorbing species, L_s, was measured geometrically and also determined experimentally by measuring the absorption coefficient of known concentrations of O_3 at 532 nm. The O_3 absorption cross section at 532 nm is well-known, 2.78×10^{-21} cm^2 $molecule^{-1}$,[30] and the O_3 concentration in the gas flow was measured via UV absorption at 254 nm before and after the CRD reactor. A value of $L_s = 4.7 \pm 0.1$ cm was obtained under the gas flow conditions typically used in the CH_3CO experiments (the CRD mirror purge flows were 25 sccm, which prevented the gas in the reactor from diffusing toward the CRD mirrors), in good agreement with the 4.7 cm geometric path length. The O_3 absorption spectrum between 530 and 550 nm was also measured and found to be in excellent agreement with the known shape of the spectrum.[30] The path length calculated using absorption coefficient data over this entire wavelength range agreed with that obtained at 532 nm. The measured absorption coefficients, $\alpha(\lambda)$, varied linearly with O_3 concentrations between 0.2×10^{15} and 1.2×10^{15} molecule cm^{-3}. The path length was insensitive to changes in pressure and flow rate through the reaction cell but decreased slightly with increasing CRD mirror purge flow, as anticipated. For example, a value of $L_s = 4.4$ cm was obtained when the CRD mirror purge flow was increased to 100 sccm.

The concentration of the photolysis precursors H_2O_2, O_3, acetone, MEK, and biacetyl in the gas flow were measured prior to the reactor by UV absorption. The precursor concentration inside the reactor was calculated from the absorption measurements and factors to account for sample dilution and differences in pressure between the absorption cells and reactor. In some cases, the O_3 concentration in the reactor was also measured directly, using CRD measurements of its absorption in the Chappius band.

The total gas flow rate through the photolysis reactor was typically 2500 sccm at total pressures in the range 60−500 Torr. To ensure that a fresh sample was present for each photolysis laser pulse, experiments were performed with a laser repetition rate of 3 Hz. Experiments performed with a slower repetition rate, 2 Hz, yielded identical measured absorption coefficient data. However, measurements made at 10 Hz showed the

influence of the photolysis of the gas mixture with multiple laser pulses, for example O_3 loss.

2.2.2. Collinear Pulsed Laser Photolysis−Cavity Ring-Down Setup. This setup is shown in Figure 1 and was described in detail in a recent publication.[15] This setup was used to measure the CH_3CO visible absorption spectrum between 600 and 650 nm and a rate coefficient for the $CH_3CO + O_2 + M$ reaction.

The apparatus used a stainless steel reaction tube ($L_s = 63$ cm) with highly reflective mirrors in the visible (>99.99%; 600−650 nm) that also have >90% transmission in the ultraviolet (290−350 nm). These mirrors also acted as the windows through which the photolysis beam was passed. Typical empty cell ring-down time constants were ~30 μs. The probe beam was from the attenuated fundamental output of a Nd:YAG laser pumped dye laser in the wavelength range 600−650 nm. The photolysis light at either 310 or 340 nm was the frequency-doubled output of a second Nd:YAG laser pumped dye laser. The photolysis beam was coupled into the reaction cell collinear to the probe beam but in the opposite direction. The photolysis laser fluence was 5−10 mJ cm^{-2} $pulse^{-1}$ inside the cell. The overlap of photolysis and probe beams in this configuration maximizes the absorption path length, L_s, and therefore the sensitivity for detection of CH_3CO.

Spectra were measured between 600 and 650 nm with CH_3CO produced from the pulsed laser photolysis of a $Cl_2/CH_3C(O)H$ mixture at 340 nm, acetone at 310 nm, and MEK at 310 nm at a total pressure of 250 Torr with N_2 as the bath gas. Pulsed laser photolysis of acetone and MEK at 310 nm were used to produce CH_3CO radicals in the determination of k_1(298 K, M) in 340 Torr N_2. The CH_3CO radical concentration in the spectrum and kinetic measurements was estimated to be ~1×10^{12} molecule cm^{-3}. The lasers were operated with a repetition rate of 2 Hz for the rate coefficient measurements, to enable the sample in the cell to be completely flushed out between laser pulses, and at 10 Hz for the spectrum measurements.

2.2.3. Discharge Flow−Cavity Ring-Down Setup. This setup is shown in Figure 1 and was used to record CH_3CO absorption spectra between 490 and 660 nm with reaction 5 as the CH_3CO radical source. A Pyrex flow tube with a 1 in. i.d. was connected near one end of the CRD cell. The gas flow from the flow tube passed through the length of the CRD cell after a small dilution from the mirror purge flow. The total pressure was <10 Torr (He) and the residence time of the gases in the CRD cell was <0.1 s. Cl atoms were produced in a sidearm of the flow tube reactor using a microwave discharge of a mixture of 0.27% Cl_2 in He. The Cl_2 concentration was determined from measured flows and pressures. Acetaldehyde was added downstream of the Cl atom source through a movable injector. The acetaldehyde concentration was measured by UV absorption before entering the flow tube and was present in large excess, ~1×10^{16} molecule cm^{-3}, of $[Cl]_0$. The initial Cl atom concentration was estimated to be ~10^{14} molecule cm^{-3}. The maximum CH_3CO absorption signal was obtained with $CH_3C(O)H$ added just prior to the gas flow entering the CRD cell (i.e., reaction 5 occurred in the CRD cell).

The reactivity of the CH_3CO radical limited its maximum average column concentration. The primary loss of CH_3CO was from self-reaction

$$CH_3CO + CH_3CO \rightarrow \text{products} \qquad (9)$$

where $k_9(298\ K) = 1.8 \times 10^{-11}$ cm^3 $molecule^{-1}$ s^{-1}.[17] Reaction of CH_3CO with Cl_2, which was present in high concentration,

$$CH_3CO + Cl_2 \rightarrow CH_3C(O)Cl + Cl \qquad (10)$$

where $k_{10}(298\ K) = 2.4 \times 10^{-11}$ cm^3 $molecule^{-1}$ s^{-1},[17] does not lead to a net loss of CH_3CO due to CH_3CO re-formation by reaction 5a and therefore did not limit the CH_3CO concentration in the CRD optical path. We estimate that the average concentration of CH_3CO along the optical path was ~2×10^{12} molecule cm^{-3}.

The CH_3CO spectrum was measured using wavelength scans with all gases flowing through the cell and the microwave discharge turned on or off. The flow of Cl_2 and acetaldehyde (with the microwave discharge off) did not produce any measurable absorption signal. The 10 Hz CRD probe beam was taken from a 308 nm excimer laser pumped dye laser and was tuned over the range 490−660 nm using several different laser dyes. The CH_3CO spectrum between 490 and 660 nm was constructed by repeating the measurements in the different wavelength regions under the same flow conditions.

2.3. Rate Coefficient Measurements. The rate coefficients for the reaction of CH_3CO with O_2, reaction 1, and O_3

$$CH_3CO + O_3 \rightarrow \text{products} \qquad (11)$$

were measured to aid the identification of the absorbing species as CH_3CO. The rate coefficient measurements were limited in scope but are sufficient to help identify the reactive species. More exhaustive measurements of the rate coefficients for reactions 1 and 11 are presently underway in our laboratory.

Rate coefficients for reaction 1 were measured under pseudo-first-order conditions in CH_3CO, $[O_2] \gg [CH_3CO]$. The initial CH_3CO concentrations, $[CH_3CO]_0$, were $< 3 \times 10^{12}$ molecule cm^{-3}, as determined from the measured absorption coefficients and the CH_3CO absorption cross section determined here. CH_3CO radicals were produced from the 310 nm photolysis of MEK and the 310 and 248 nm photolysis of acetone. CH_3CO temporal profiles were determined using the absorption coefficients measured at 532 and 610 nm and obeyed

$$\ln\left(\frac{[CH_3CO]_t}{[CH_3CO]_0}\right) = \ln\left(\frac{\alpha_t}{\alpha_0}\right) = -(k_1[O_2] + k_d) = -k't \qquad (12)$$

where k' is the pseudo-first-order rate coefficient and k_d is the first-order rate coefficient measured in the absence of O_2. k_d represents the loss of CH_3CO radicals due to reactions with impurities in the bath gas, and background O_2 as well as diffusion of CH_3CO out of the detection volume. All of these processes are assumed to be first order in $[CH_3CO]$. Typical values of k_d were between 250 and 400 s^{-1}. k' was measured for a range of O_2 concentrations, $(0.3-2.7) \times 10^{15}$ molecule cm^{-3}, and k_1(298 K, M) was determined from the slope of a plot of k' vs $[O_2]$. k_1(298 K, M) was measured in 60 Torr He and 340 Torr N_2.

The rate coefficient for the reaction of CH_3CO with O_3, reaction 11, at 298 K was also measured. CH_3CO radicals were produced following the 248 nm pulsed laser photolysis of an O_3/H_2O mixture in a He bath gas

$$O_3 + h\nu \rightarrow O(^1D) + O_2(^1\Delta) \qquad (13a)$$

$$\rightarrow O(^3P) + O_2(^3\Sigma) \qquad (13b)$$

$$O(^1D) + H_2O \rightarrow 2OH \qquad (14)$$

in the presence of a large excess of acetaldehyde.

$$OH + CH_3C(O)H \rightarrow H_2O + CH_3CO \qquad (4)$$

We determined $k_{11}(298\ K) = (4.2 \pm 1.0) \times 10^{-11}$ cm^3 molecule^{-1} s^{-1} (quoted uncertainty is at the 2σ level including estimated systematic errors), in agreement with the literature value of $(4.7 \pm 1.0) \times 10^{-11}$ cm^3 molecule^{-1} s^{-1}.[20] Further details of our rate coefficient measurements for reaction 11 and its temperature dependence are presented elsewere.[31]

2.4. CH_3CO Cross Section Determinations. Cross sections for the visible absorption spectrum of the CH_3CO radical were determined using

$$\alpha(\lambda) = [CH_3CO]\sigma_{CH_3CO}(\lambda) = [P]\sigma_P(248\ nm)\,\Phi_P\Phi_R F\sigma_{CH_3CO}(\lambda) \quad (15)$$

where P is the OH precursor, either H_2O_2 or O_3, $\sigma_P(248\ nm)$ is the absorption cross section of the precursor at 248 nm, Φ_P is the OH yield (2 for H_2O_2 and 1.8 for O_3),[24] Φ_R is the CH_3CO yield in reaction 4 (0.95[26]), and F is the photolysis laser fluence (photons cm^{-2} pulse^{-1}). The CH_3CO absorption cross section, $\sigma_{CH_3CO}(\lambda)$, is determined from the slope of $\alpha(\lambda)$ versus $[CH_3CO]_0$ and the photolysis laser fluence.

The 248 nm pulsed laser photolysis of O_3/H_2O mixtures, reactions 13 and 14, in a He bath gas or H_2O_2

$$H_2O_2 + h\nu \rightarrow 2OH \quad (16)$$

was used to produce known amounts of OH radicals in the presence of excess acetaldehyde. Two independent methods were used to determine the photolysis laser fluence and calibrate the power meter used to monitor the photolysis laser fluence. The primary calibration standard was the 248 nm photolysis of ozone. These experiments were performed in a N_2 bath gas to rapidly quench the $O(^1D)$ produced by photolysis to $O(^3P)$,

$$O(^1D) + N_2 \rightarrow O(^3P) + N_2 \quad (17)$$

where $k_{17}(298\ K) = 2.6 \times 10^{-11}$ cm^3 molecule^{-1} s^{-1},[24] and prevent secondary reactive losses of O_3 on the time scale of the measurement. The fraction of ozone lost via photolysis was measured using CRD measurements at 532 nm under conditions identical to those used in the CH_3CO cross section measurements. This internal calibration method, therefore, has the advantage that both the calibration and cross section measurements were performed using the same apparatus and methods. Calibrations were made with initial ozone concentrations in the range $(0.3-5) \times 10^{14}$ molecule cm^{-3} and laser fluences between 2 and 15 mJ cm^{-2} pulse^{-1}.

The second fluence calibration method used 248 nm photolysis of acetone. The method is similar to that described in previous work from our laboratory.[11] Basically, acetone/N_2 samples are photolyzed with multiple photolysis laser pulses in a small volume cell while the laser fluence is monitored with a power meter. The loss of acetone per laser shot was determined off-line using Fourier transform infrared spectroscopy. The laser fluence calibrations obtained using the ozone and acetone photolysis methods agreed to within 10%. An average calibration factor from the two methods was used in the CH_3CO data analysis.

2.5. Materials. He (UHP, 99.999%) and N_2 (UHP, >99.99%) were used as bath gases and O_2 (UHP, >99.99%) was used as a reactant in the kinetic measurements. Cl_2 was taken from a commercially prepared 0.27% Cl_2 in UHP He mixture. Samples of acetone (>99.9%), methyl ethyl ketone ($CH_3C(O)CH_2CH_3$, >99%), biacetyl ($CH_3C(O)C(O)CH_3$, >99%), and acetaldehyde ($CH_3C(O)H$, >99.5%) were degassed using freeze−pump−thaw cycles prior to use and stored under vacuum in Pyrex reservoirs with Teflon stopcocks. Samples were introduced into the gas flow by passing a small flow of bath gas over the liquid surface of the precursor prior to dilution with the main gas flow and entering the reactor. The sample reservoirs were kept in constant temperature baths to stabilize the sample flow out of the reservoir. Concentrated H_2O_2 (>95%, as determined by titration with a standard $KMnO_4$ solution) was prepared by bubbling N_2 through a H_2O_2 sample, initially at ~60 wt %, for several days prior to use. H_2O_2 was introduced to the gas flow by bubbling a small flow of He, approximately 1% of the total gas flow, through the >95% pure liquid H_2O_2 sample. Ozone was prepared by passing O_2 through a commercial ozonizer and stored on silica gel at 195 K. A dilute mixture of O_3 in He (~0.1% mole fraction) was prepared from this sample in a darkened 12 L Pyrex bulb. Flow from the bulb or a flow of He through the ozone silica gel trap were used to introduce ozone into the gas flow of the apparatus.

The concentrations of O_3, H_2O_2, acetone, MEK, and biacetyl were measured in situ by UV absorption. The O_3 concentration was also measured in the reactor by CRDS in some cases. UV absorption measurements were made using a Hg pen-ray lamp light source at either 184.9 nm or 253.7 nm isolated using narrow bandpass filters and detected by a photodiode. The absorption cells were made from 1 in. diameter Pyrex tubing fitted with quartz windows. Absorption cells with pathlengths of 10, 25, 50, and 100 cm were used in the measurements depending on the species and concentration range being used.

The absorption cross sections for acetone, MEK, and biacetyl at 184.9 nm were determined as part of this work. For the cross section measurements, dilute mixtures of acetone, MEK, and biacetyl in He (~0.5% mole fraction) were prepared manometrically. The absorbance of the compound was measured using a 20 cm long absorption cell and the concentration of the compound determined from the pressure. The measured absorbance obeyed Beer's law and yielded absorption cross sections of 2.91×10^{-18}, 1.31×10^{-18}, 1.46×10^{-18} (in units of cm^2 molecule^{-1}, base e) for acetone, MEK, and biacetyl, respectively. The uncertainty in the cross section values is estimated to be ~4% at the 2σ level. The absorption cross sections for these compounds and for O_3 and H_2O_2 at other wavelengths were taken from the literature.[11,24,32,33] The concentrations of Cl_2 and O_2 were determined using measured flow rates and pressures.

Gas flow rates were measured using calibrated electronic mass flow transducers. Pressures were measured using 100 and 1000 Torr capacitance manometers. All experiments were performed at room temperature, ~298 K.

3. Results and Discussion

The absorption spectra of CH_3CO measured using the different CH_3CO sources over the wavelength range 490−660 nm are shown in Figure 2. The spectra include results obtained using a range of experimental conditions, three different experimental apparatus and five sets of CRD mirrors. Overlapping wavelength regions were scanned whenever possible to improve the consistency in the overall spectrum measurement. The majority of the spectrum measurements using the photochemical sources (acetone, MEK, and biacetyl) were made in back-to-back experiments to reduce possible systematic errors in the measurements.

The absorption spectra obtained using the photolysis methods were recorded with a 100 μs delay between the photolysis and probe laser pulses. Spectra recorded with longer delays had the

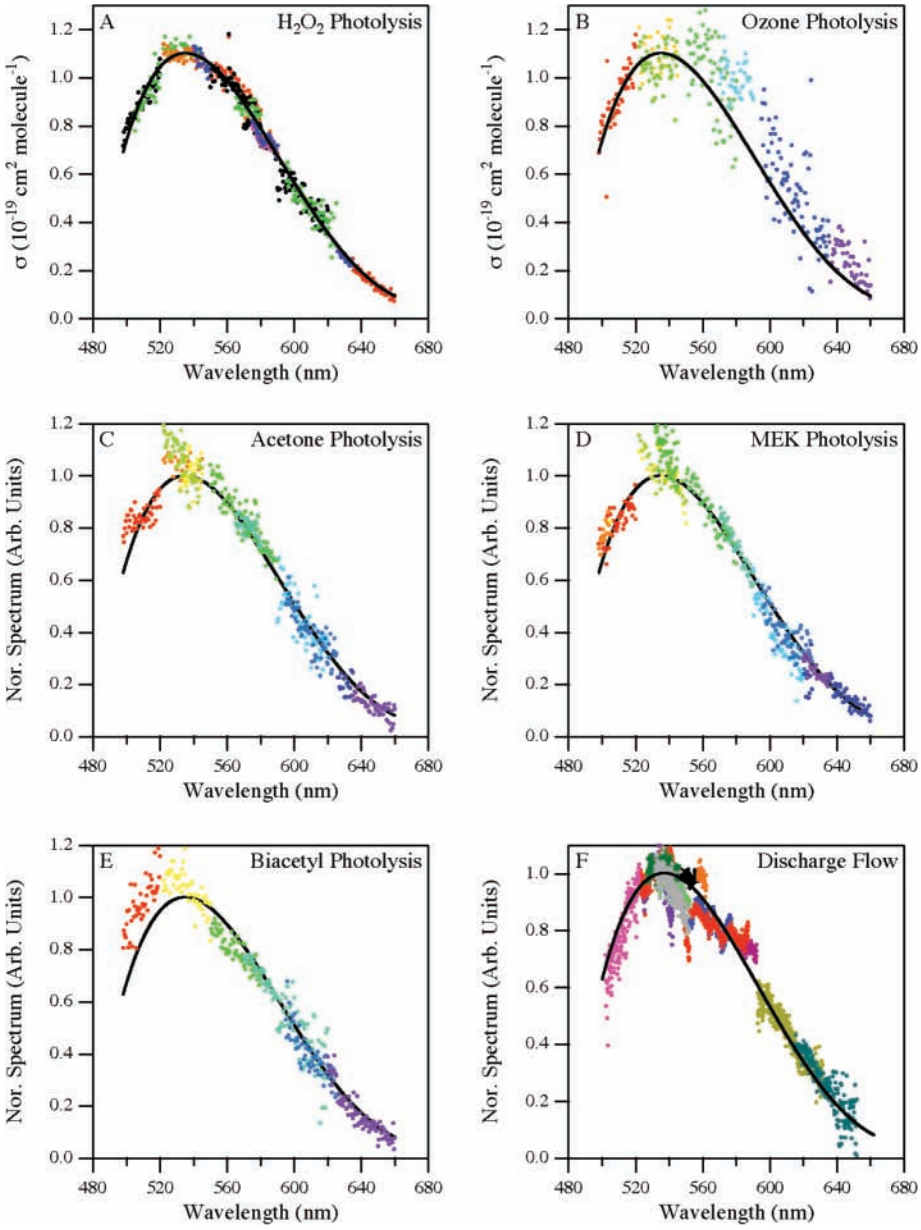

Figure 2. Gas-phase CH_3CO absorption spectra measured using cavity ring-down spectroscopy with various CH_3CO sources (as labeled). The different colors represent independent sets of measurements performed with various combinations of experimental conditions and sets of CRD mirrors. The solid lines are from a polynomial fit to the spectrum obtained using the H_2O_2 photolysis source to produce CH_3CO. The CH_3CO spectra obtained using the H_2O_2 and O_3 sources have been normalized to the CH_3CO absorption cross at 532 nm determined in this work, 1.1×10^{-19} cm^2 molecule^{-1} (see text for details). The measured CH_3CO spectra from the other sources have been normalized to unity at 532 nm.

same shape as those shown in Figure 2 but had weaker signals due to lower CH_3CO concentration. We conclude from these measurements that CH_3CO was either vibrationally thermalized or that vibrational excitation of CH_3CO does not significantly influence the shape of the spectrum. The measured absorption spectra are continuous with a broad peak at 535 nm and no apparent ro-vibrational structure. Spectra recorded by stepping the dye laser in 0.1 nm increments were the same as those obtained in 0.5 nm increments.

We have used the spectrum obtained with the H_2O_2 photolysis source, Figure 2A, as a reference for comparison to the spectra obtained with the other CH_3CO sources. The solid line shown in Figure 2A was obtained by fitting the spectrum to the polynomial

$$\sigma_{CH_3CO}(\lambda) = A + B\lambda + C\lambda^2 + D\lambda^3 + E\lambda^4 \qquad (18)$$

TABLE 1: Parameters Used To Fit the CH_3CO Visible Absorption Spectrum between 490 and 660 nm to $\sigma_{CH_3CO}(\lambda) = A + B\lambda + C\lambda^2 + D\lambda^3 + E\lambda^4$ (σ in Units of cm^2 molecule^{-1} (base e) and λ in nm)

coefficient	value
A	-6.6124×10^{-17}
B	4.1947×10^{-19}
C	-9.865×10^{-22}
D	1.02141×10^{-24}
E	-3.93411×10^{-28}

The fit reproduces the experimentally determined spectrum very well, and the fit coefficients are given in Table 1. Fits using other functional function forms, such as a simple Gaussian equation, do not reproduce the spectrum within the precision of the experimental data. The parametrization is only valid over the wavelength range of the experimental data, 490−660 nm, but provides a convenient method to reproduce the CH_3CO spectrum. The fit is reproduced in the other panels in Figure 2

(normalized at the peak of the measured spectra) to provide a visual comparison of the spectra obtained with the various CH_3CO sources.

The shapes of the spectra obtained with each CH_3CO source are in good agreement. The spectrum obtained with the ozone source, Figure 2B, is, however, of lower signal-to-noise as a result of the rapid reaction of O_3 with the absorbing species, reaction 11, where $k_{11}(298\ K) = (4.7 \pm 1.0) \times 10^{-11}$ cm^3 molecule^{-1} s^{-1}.[20] Measurements made with $[O_3]_0$ greater than $\sim 2 \times 10^{14}$ molecule cm^{-3} yielded nonexponential ring-down profiles, consistent with the loss of CH_3CO radicals during the cavity ring-down time. Low $[O_3]_0$, and therefore lower CH_3CO radical concentrations, were required to avoid nonexponential ring-down profiles.

The absorption spectra measured following the 248 nm photolysis of acetone, MEK, and biacetyl, Figure 2C−E, are also in agreement with the empirical fit. The largest deviations in the spectra (~10% too high) are in the wavelength region between 490 and 540 nm. As mentioned earlier, the 248 nm photolysis of MEK, reaction 6, could produce CH_3CO, CH_3CH_2CO or a combination of these radicals. Khamaganov et al.[6] recently reported pressure dependent CH_3 quantum yields following the 248 nm photolysis of MEK. Quantum yields varied from 0.45, in the low-pressure limit, to ~0.2 for pressures >700 Torr. Therefore, at the pressures used in the present MEK experiments, 60 Torr, both CH_3CO and CH_3CH_2CO radicals are formed. It is reasonable to expect that the absorption spectra of the CH_3CO and CH_3CH_2CO radicals would be similar. Therefore, it is not possible to assign the spectrum to CH_3CO based solely on the spectrum measurements using the MEK source. Rate coefficient measurements were performed as part of this work, as described in the next section, to aid this assignment. Spectral measurements (although not performed in this study) following the UV photolysis of diethyl ketone (DEK, $CH_3CH_2C(O)CH_2CH_3$), which should be an unambiguous source of the CH_3CH_2CO radical, would aid the spectrum analysis.

Several complications were encountered when using the discharge flow method that increased the scatter/noise in these measurements, particularly at wavelengths <580 nm. UV and VUV light emitted from the microwave discharge reaching the CRD mirrors caused drifts in mirror reflectivity during the experiment. This affect primarily contributed to the uncertainty in τ_0 used to calculate CH_3CO absorption coefficients in the spectrum measurements. In addition, spectral scans made with the $CH_3C(O)H$ precursor flow turned off, but the microwave discharge and Cl_2 on, showed diffuse structured absorption features at wavelengths <580 nm. The structured absorption was not observed when $CH_3C(O)H$ was present. The absorbing species was not identified, but its presence contributed to the uncertainty in τ_0 and the CH_3CO absorption coefficient. Nevertheless, the spectrum obtained using the discharge flow method is similar to that obtained using the other methods.

The spectrum obtained using the collinear PLP-CRD setup between 600 and 650 nm is included in Figure 2F. We have normalized the CH_3CO spectrum from the collinear PLP-CRD experiments to the results obtained from the discharge flow method in this wavelength region. The shape of the spectra is in good agreement with that obtained using the other methods.

3.1. Rate Coefficient Measurements. The measured pseudo-first-order rate coefficient, k', data obtained for the reaction of the absorbing species with O_2 is shown in Figure 3. Rate coefficients were measured at total pressures of 60 Torr (He) and 340 Torr (N_2) at 298 K. The temporal decays of the absorbing species followed the rate law given in eq 12. At longer reaction times, >10 ms, the measured time constant returned to its pre-photolysis value, τ_0. This observation indicates that no long-lived absorbing species were present. k_1(M) measured using the 310 nm photolysis of acetone or MEK as the CH_3CO radical source agreed within the combined uncertainties of the measurements. In addition, k_1(M) measured using two different probe wavelengths (532 and 610 nm) were the same. A weighted linear least-squares fit to the data given in Figure 3 yields $k_1(298\ K, 60\ Torr\ (He)) = (3.2 \pm 0.3) \times 10^{-12}$ cm^3 molecule^{-1} s^{-1} and $k_1(298\ K, 340\ Torr\ (N_2)) = (3.8 \pm 0.3) \times 10^{-12}$ cm^3 molecule^{-1} s^{-1} where the uncertainties are 2σ of the fit precision. These values are in good agreement with the rate coefficients reported by Blitz et al.[2] and Tyndall et al.[1] for reaction 1 (after scaling the Tyndall et al. values by a factor of 1.8 to account for the revised rate coefficient for the $CH_3CO + Cl_2$ reaction[34]). Romero et al.[35] reported a rate coefficient for the $CH_3CH_2CO + O_2 + M$ reaction of 5.3×10^{-12} cm^3 molecule^{-1} s^{-1}, independent of pressure between 5 and 400 Torr (He). On the basis of their measured rate coefficient and literature values for k_1(298 K, M), Romero et al. deduced that CH_3CO is formed almost exclusively, >80%, over the CH_3CH_2CO radical in the 248 nm photolysis of MEK. Our results and the recent CH_3 quantum yield measurements of Khamaganov et al.[6] support this conclusion.

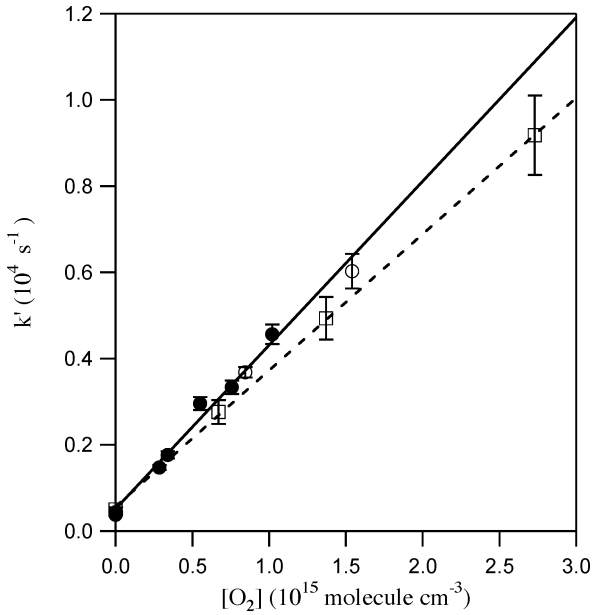

Figure 3. Measured pseudo-first-order rate coefficient data for the reaction of the absorbing species (CH_3CO) with O_2, $CH_3CO + O_2 + M \rightarrow$ products, at 298 K. Measurements were made at total pressures of 60 Torr He (squares) and 340 Torr N_2 (circles). The 340 Torr data was obtained using 310 nm pulsed laser photolysis of acetone (solid circles) and methyl ethyl ketone (open circles) as the CH_3CO radical source with a CRD probe wavelength of 610 nm. The 60 Torr data were obtained using 248 nm pulsed laser photolysis of acetone as the CH_3CO radical source with a CRD probe wavelength of 532 nm. The lines are the weighted least-squares fits to the data yielding $k_1(60\ Torr) = (3.2 \pm 0.3) \times 10^{-12}$ cm^3 molecule^{-1} s^{-1} and $k_1(340\ Torr) = (3.8 \pm 0.3) \times 10^{-12}$ cm^3 molecule^{-1} s^{-1}, where the uncertainties are 2σ of the fit precision.

The agreement between the shape of the absorption spectrum measured with each of the different CH_3CO sources and the agreement of our measured values for k_1(298 K, M) and k_{11}(298 K) with literature values gives us confidence that the absorbing species is indeed CH_3CO. Therefore, we have assigned the measured absorption spectrum to the CH_3CO radical. We note that our CH_3CO spectrum is not consistent with the theoretical

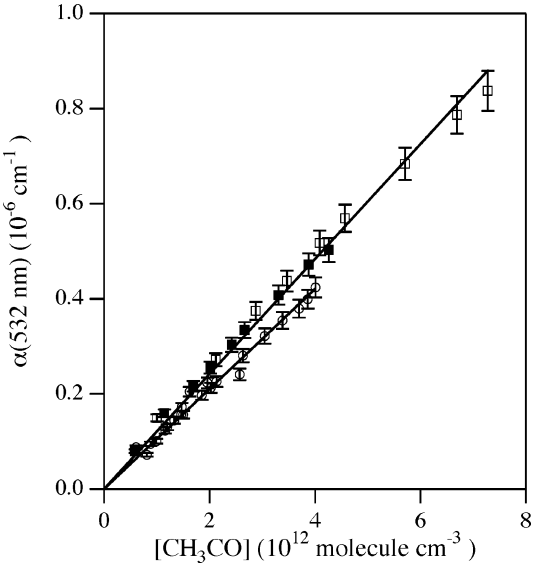

Figure 4. Determination of the CH_3CO absorption cross section at 532 nm. Cross sections were determined from the slope of α(532 nm) versus [CH_3CO] and the calibrated photolysis laser fluence, eq 15. Cross sections were determined using 248 nm photolysis of O_3 or H_2O_2 to produce OH radicals for reaction 4 (see text for details). The linear least-squares fit to the data obtained using the O_3 source (open circles) yields $\sigma_{CH_3CO}(532\text{ nm}) = (1.05 \pm 0.03) \times 10^{-19}$ cm^2 molecule^{-1}. For the H_2O_2 source, measurements made using photolysis laser fluences of 7.25 mJ cm^{-2} pulse^{-1} (solid squares) and 12.5 mJ cm^{-2} pulse^{-1} (open squares) are in good agreement. A linear least-squares fit to all the data yields $\sigma_{CH_3CO}(532\text{ nm}) = (1.21 \pm 0.03) \times 10^{-19}$ cm^2 molecule^{-1}. The quoted uncertainties are the 2σ value from the fit precision.

study that predicted an excitation energy for the $A^2A'' \leftarrow X^2A'$ transition of 60 kcal mol^{-1} (476 nm).[16] Our measured CH_3CO spectrum (a peak at 535 nm, 53.4 kcal mol^{-1}) suggests a lower transition energy. Recent theoretical calculations by Marshall,[36] obtained with coupled-cluster theory extrapolated to the infinite basis set limit, yields an excitation energy of 55.5 kcal mol^{-1} (515 nm) that is closer to the observed peak of the experimental spectrum. The theoretical studies also find the A^2A'' excited state to be bound. However, the lack of structure in our CH_3CO spectrum indicates a short excited-state lifetime either via dissociation or coupling.

3.2. CH_3CO Absorption Cross Section. The cross sections for the CH_3CO absorption spectrum were determined using reaction 4 as the source of CH_3CO and 248 nm photolysis of H_2O_2 and O_3/H_2O as the source of OH radicals. Absorption cross sections were determined from CRD measurements at 532 nm and during the course of scanning the absorption spectrum. The agreement between these two data sets is excellent.

The CH_3CO absorption cross section was obtained from a plot of the absorption coefficient, $\alpha(\lambda)$, versus $[CH_3CO]_0$. Examples of data used in the cross section determination are shown in Figure 4. Linear least-squares fits to the data shown in Figure 4 yield $\sigma_{CH_3CO}(532\text{ nm})$ values of $(1.05 \pm 0.03) \times 10^{-19}$ cm^2 molecule^{-1} and $(1.20 \pm 0.03) \times 10^{-19}$ cm^2 molecule^{-1}, for the O_3 and H_2O_2 sources, respectively. The quoted errors are the 2σ level (95% confidence) values from the precision of the fit. These two values were the largest and smallest CH_3CO absorption cross sections determined in our experiments. The measured absorption coefficient varied linearly with respect to the initial precursor concentration and laser fluence (varied by a factor of 2) over the range of values used in the measurements. We report an average $\sigma_{CH_3CO}(532\text{ nm})$ value of 1.1×10^{-19} cm^2 molecule^{-1} with an estimated uncertainty of $\pm$15% (see Error Analysis section). The CH_3CO spectra shown in Figure 2A,B were normalized at 532 nm to this value.

3.3. Error Analysis. In this section, we present a general discussion of the uncertainties associated with the determinations of the CH_3CO absorption spectrum and its absorption cross section. The best way to evaluate the uncertainty in the shape of the CH_3CO spectrum is through the comparison of the spectra obtained using the different CH_3CO sources shown in Figure 2. Spectra obtained in the overlapping wavelength regions were in good agreement (better than 5%), indicating the self-consistency of the CH_3CO spectra measurements. An examination of the spectra shows a few minor discrepancies among the spectra as pointed out earlier. For example, the spectra obtained using the O_3 source for wavelengths >550 nm are systematically higher than others. As noted earlier, the precision of the measurements obtained with this source were, however, lower than obtained with the other CH_3CO sources. The spectral measurements obtained with the biacetyl photolysis source are also systematically high for wavelengths <520 nm. On the basis of the level of agreement among the measured spectra, we estimate the uncertainty in the ratio $\sigma(\lambda)/(\sigma(532\text{ nm}))$ to be ~10%. Resolving further details in the shape of the spectrum will hopefully be addressed in future work on the spectroscopy of the CH_3CO radical.

The uncertainty in the CH_3CO absorption cross sections can be estimated through the parameters used in eq 15 and the differences obtained when using the two different CH_3CO sources. We estimate the uncertainty in L_s to be ~0.1 cm, ~2%. Uncertainties in the gas flow, pressure, and determination of the ring-down time constant are small, and they did not contribute significantly to the overall uncertainty, <5%. The concentrations of the photolysis precursors were measured by UV absorption, both before and after the CRD reactor, and in the reactor in the case of O_3, whenever possible. The accuracy of the precursor concentration was known to better than a few percent. The UV absorption measurements before and after the reactor yielded precursor concentrations that agreed within 5%. The absorption cross sections for the precursors also contribute to the overall uncertainty. The uncertainty in the cross sections partially cancels in eq 15 because they were used in the concentration determination and for the determination of the fraction of precursor photolyzed. The ratios of the absorption cross sections at different wavelengths are expected to be known better than the absolute values, and we estimate the contribution of the uncertainty to the overall error in cross section to be on the order of ~5%.

The photolysis laser fluence used in eq 15 represents the single largest source of uncertainty in the cross section determination. Two methods were used to calibrate the laser fluence and they agreed to within 10%. In addition, the photolysis fluence along the optical path, L_s, was measured to be uniform. The CH_3CO absorption cross section was determined multiple times during the course of the study. The precision of these independent measurements was good, <5% uncertainty, as shown in Figure 4. By combining the uncertainties in the precision of the cross section determinations, the photolysis laser fluence, precursor concentration, and estimated systematic errors, we estimate the uncertainty in the CH_3CO absorption cross section at 532 nm to be 15% at the 1σ level. The absolute CH_3CO absorption cross sections at wavelengths away from the peak of the spectrum have a similar level of uncertainty.

4. Conclusions

The visible absorption spectrum of the CH_3CO radical was identified and quantified in this study. The measured absorption spectrum was assigned to the CH_3CO radical on the basis of the consistency of the spectral shape from different chemical and photolytic sources of the CH_3CO radical and the agreement of measured rate coefficients for the $CH_3CO + O_2 + M$ and $CH_3CO + O_3$ reactions with literature values. The CH_3CO absorption spectrum between 490 and 660 nm has a broad peak centered near 535 nm and shows no discernible structure. The absorption cross section at 532 nm was determined to be $(1.1 \pm 0.2) \times 10^{-19}$ cm^2 molecule^{-1}.

The characterization of the visible absorption spectrum of the CH_3CO radical is important to both theoretical and experimental studies. Comparison of the CH_3CO $A^2A'' \leftarrow X^2A'$ absorption spectrum with results from theoretical calculations will improve our understanding of the excited electronic states of this important atmospheric radical. The characterization of the CH_3CO visible absorption spectrum also enables laboratory kinetic and photochemical studies. For example, measurements of the CH_3CO quantum yield following the photolysis of acetone, methyl ethyl ketone (MEK), and biacetyl at 248 nm[29] as well as the rate coefficient for the reactions of CH_3CO with O_2, O_3, and Cl_2 are currently being studied in our laboratory using results obtained in the present study.

Acknowledgment. This work was supported in part by the NASA's Atmospheric Composition Program.

References and Notes

(1) Tyndall, G. S.; Orlando, J. J.; Wallington, T. J.; Hurley, M. D. *Int. J. Chem. Kinet.* **1997**, *29*, 655.

(2) Blitz, M. A.; Heard, D. E.; Pilling, M. J. *Chem. Phys. Lett.* **2002**, *365*, 374.

(3) Talukdar, R. K.; Burkholder, J. B.; Schmoltner, A.-M.; Roberts, J. M.; Wilson, R. R.; Ravishankara, A. R. *J. Geophys. Res.* **1995**, *100*, 14163.

(4) McKeen, S. A.; Gierczak, T.; Burkholder, J. B.; Wennberg, P. O.; Hanisco, T. F.; Keim, E. R.; Gao, R.-S.; Liu, S. C.; Ravishankara, A. R.; Fahey, D. W. *Geophys. Res. Lett.* **1997**, *24*, 3177.

(5) Arnold, S. R.; Chipperfield, M. P.; Blitz, M. A.; Heard, D. E.; Pilling, M. J. *Geophys. Res. Lett.* **2004**, *31*, L07110, doi: 10.1029/2003GL019099.

(6) Khamaganov, V.; Karunanandan, R.; Rodriguez, A.; Crowley, J. N. *Phys. Chem. Chem. Phys.* **2007**, doi: 10.1039/b701382e.

(7) Somnitz, H.; Fida, M.; Ufer, T.; Zellner, R. *Phys. Chem. Chem. Phys.* **2005**, *7*, 3342, doi: 10.1039/b506738c.

(8) Blitz, M. A.; Heard, D. E.; Pilling, M. J. *J. Phys. Chem. A* **2006**, *110*, 6742.

(9) Blitz, M. A.; Heard, D. E.; Pilling, M. J.; Arnold, S. R.; Chipperfield, M. P. *Geophys. Res. Lett.* **2004**, *31*, L06111, doi: 10.1029/2003GL018793.

(10) Emrich, M.; Warneck, P. *J. Phys. Chem. A* **2000**, *104*, 9436.

(11) Gierczak, T.; Burkholder, J. B.; Bauerle, S.; Ravishankara, A. R. *Chem. Phys.* **1998**, *231*, 229.

(12) Horowitz, A. *J. Phys. Chem.* **1991**, *95*, 10816.

(13) Gardner, E. P.; Wijayaratne, R. D.; Calvert, J. G. *J. Phys. Chem.* **1984**, *88*, 5069.

(14) Lightfoot, P. D.; Kirwan, S. P.; Pilling, M. J. *J. Phys. Chem.* **1988**, *92*, 4938.

(15) Flad, J. E.; Brown, S. S.; Burkholder, J. B.; Stark, H.; Ravishankara, A. R. *Phys. Chem. Chem. Phys.* **2006**, *8*, 3636.

(16) Mao, W.; Li, Q.; Kong, F.; Huang, M. *Chem. Phys. Lett.* **1998**, *283*, 114.

(17) Maricq, M. M.; Szente, J. J. *Chem. Phys. Lett.* **1996**, *253*, 333.

(18) Cameron, M.; Sivkumaran, V.; Dillon, T. J.; Crowley, J. N. *Phys. Chem. Chem. Phys.* **2002**, *4*, 3628, doi: 10.1039/b202586h.

(19) Li, H.; Li, Q.; Mao, W.; Zhu, Q.; Kong, F. *J. Chem. Phys.* **1997**, *106*, 5943.

(20) Wang, J.; Chen, H.; Glass, G. P.; Curl, R. F. *J. Phys. Chem. A* **2003**, *107*, 10834.

(21) O'Keefe, A.; Deacon, D. A. G. *Rev. Sci. Instrum.* **1988**, *59*, 2544.

(22) Brown, S. S.; Ravishankara, A. R.; Stark, H. *J. Phys. Chem. A* **2000**, *104*, 7044.

(23) Brown, S. S.; Wilson, R. W.; Ravishankara, A. R. *J. Phys. Chem. A* **2000**, *104*, 4976.

(24) Sander, S. P.; Friedl, R. R.; Golden, D. M.; Kurylo, M. J.; Moortgat, G. K.; Wine, P. H.; Ravishankara, A. R.; Kolb, C. E.; Molina, M. J.; Finlayson-Pitts, B. J.; Huie, R. E.; Orkin, V. L. *Chemical kinetics and photochemical data for use in atmospheric studies*; JPL Pub. 06-2, Jet Propulsion Laboratory: Pasadena, 2006; Vol. Evaluation No. 15.

(25) NIST Chemistry WebBook, NIST Standard Reference Database; Vol. 69 http://webbook.nist.gov/chemistry.

(26) Butkovskaya, N. I.; Kukui, A.; Le Bras, G. *J. Phys. Chem. A* **2004**, *108*, 1160.

(27) Tyndall, G. S.; Orlando, J. J.; Wallington, T. J.; Hurley, M. D.; Goto, M.; Kawasaki, M. *Phys. Chem. Chem. Phys.* **2002**, *4*, 2189.

(28) Niki, H.; Maker, P. D.; Savage, C. M.; Breitenbach, L. P. *J. Phys. Chem.* **1985**, *89*, 588.

(29) Rajakumar, B.; Flad, J. E.; Gierczak, T.; Ravishankara, A. R.; Burkholder, J. B. *J. Photochem. Photobiol. A: Chem.*, to be submitted.

(30) Burkholder, J. B.; Talukdar, R. K. *Geophys. Res. Lett.* **1994**, *21*, 581.

(31) Gierczak, T.; Rajakumar, B.; Flad, J. E.; Ravishankara, A. R.; Burkholder, J. B. Manuscript in preparation.

(32) Martinez, R. D.; Buitrago, A. A.; Howell, N. W.; Hearn, C. H.; Joens, J. A. *Atmos. Environ.* **1992**, *26A*, 785.

(33) Horowitz, A.; Meller, R.; Moortgat, G. K. *J. Photochem. Photobiol. A: Chem.* **2001**, *146*, 19.

(34) Tyndall, G. S.; Orlando, J. J.; Kegley-Owen, C. S.; Wallington, T. J.; Hurley, M. D. *Int. J. Chem. Kinet.* **1999**, *31*, 776.

(35) Romero, M. T. B.; Blitz, M. A.; Heard, D. E.; Pilling, M. J.; Price, B.; Seakins, P. W.; Wang, L. *Faraday Discuss.* **2005**, *130*, 73.

(36) Marshall, P. Personal communication, 2006.